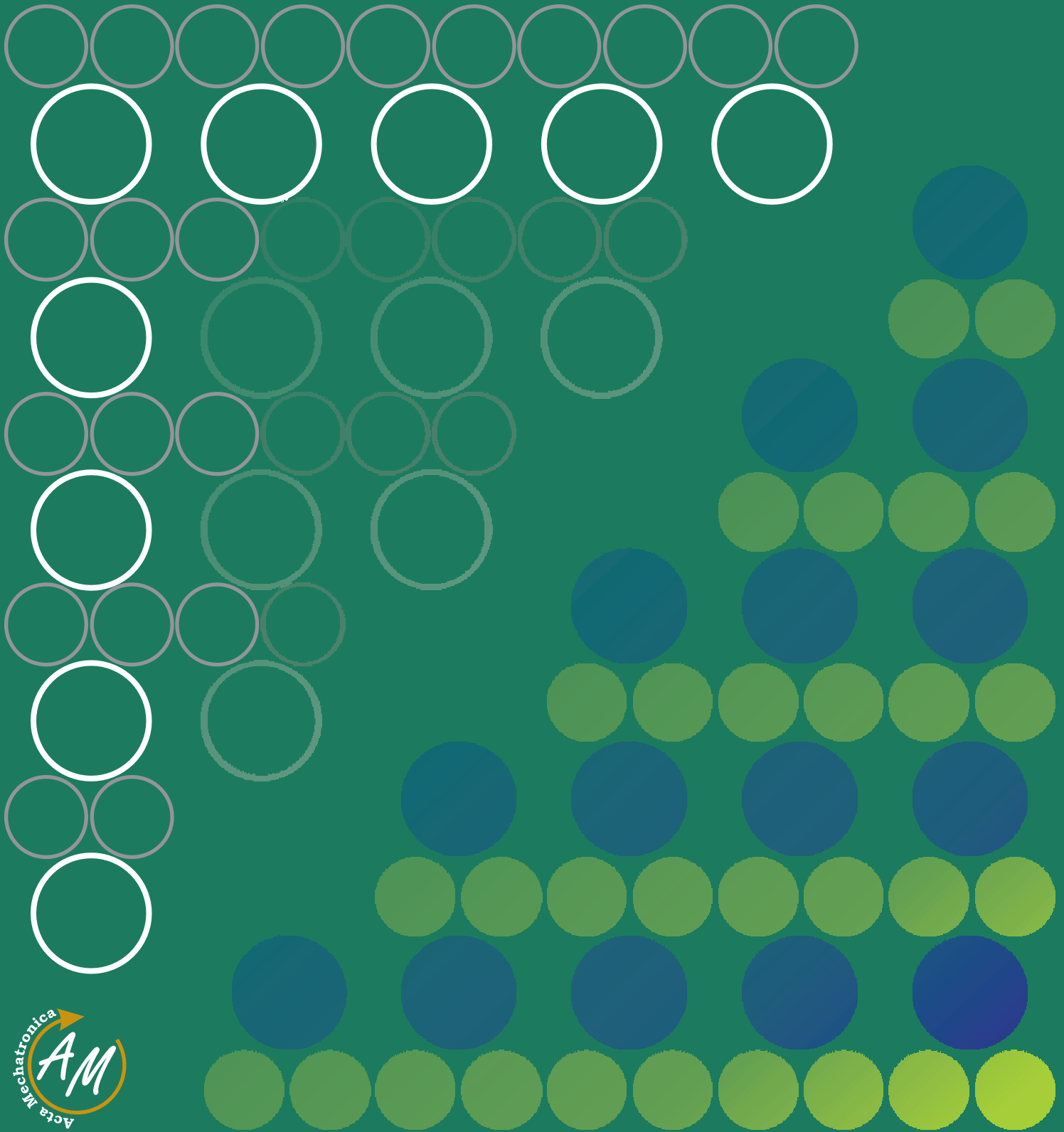


ACTA MECHATRONICA

2018 Volume 3

Issue 4



International Scientific Journal about Mechatronics
electronic journal
ISSN 2453-7306

CONTENTS
(DECEMBER 2018)

(pages 1-6)

**SELECTION OF THE CRACK DRIVING FORCE CONCEPT IN CONTEXT
OF LINEAR-ELASTIC AND ELASTICPLASTIC FRACTURE MECHANICS**

Michal Kráčalík

(pages 7-10)

SNAKE-LIKE ROBOTS

Ivan Virgala, Ľubica Miková, Michal Kelemen, Darina Hroncová

(pages 11-14)

**DESIGN OF BODY WHEEL SHAPE TO IMPROVE TEETH STIFFNESS
FOR GEARBOX OF MECHATRONIC SYSTEMS**

Silvia Medvecká-Beňová, Peter Frankovský

(pages 15-21)

**THE ASPECTS OF STRESS ANALYSIS PERFORMED BY DIGITAL IMAGE
CORRELATION METHOD RELATED WITH SMOOTHING AND ITS
INFLUENCE ON THE RESULTS**

Martin Hagara, Jozef Bocko

SELECTION OF THE CRACK DRIVING FORCE CONCEPT IN CONTEXT OF LINEAR-ELASTIC AND ELASTIC-PLASTIC FRACTURE MECHANICS

Michal Kráčalík

Untere Hauptstraße 48/5, 2424 Zurndorf, Austria,
michal.kracalik@gmail.com

Keywords: fracture mechanics, crack driving force, yielding

Abstract: Fracture mechanics is a continuum mechanics approach to describe cracks in materials. There are plenty of fracture mechanics concepts such as linear elastic fracture mechanics (LEFM), elastic-plastic fracture mechanics (E-PFM), dynamic, the time-dependent fracture mechanics that are limited to specific loading conditions, crack geometry (length) and material behaviour. Current paper evaluates applicability of a crack driving force in context of LEFM and E-PFM for arbitrary (quasi-static) loading and yielding conditions to help engineers choose appropriate fracture mechanics concept for their applications.

1. Introduction

Two fracture mechanics approaches are standardly used in LEFM – The energy release rate and the stress intensity factor. Both hold their validity for linear-elastic material behaviour or small scale yielding (SSY) conditions. The machine parts are components are normally designed for linear-elastic behaviour. Hence, the stress intensity factor is widely used concept in the mechanical engineering. Due to the overloading and local stress/strain field around notches are machine parts exposed to local plastic deformations. The E-PFM concepts are incorporated to describe behaviour of such cracks. The crack tip opening displacement (CTOD) and the J-integral require additionally lower restriction on the fracture mechanics tests as the stress intensity factor approach [1]. The cyclic CTOD can be used for characterization of a crack growth under large scale and general yielding condition under cyclic loading [2] but that approach is limited to fracture Mode I; for Mode II (or Mixed Mode) are currently investigated approaches like crack face displacement [3]. The J-integral does not characterize the real crack driving force for a crack in an elastic-plastic material behaviour even for proportional cyclic loading [2], [4]. The physically appropriate crack driving force for an elastic-plastic material behaviour has been derived [4]. Based on the configurational force concept (“modified J-integral”), the integration contour which encloses the active plastic zone characterizes the physically appropriate crack driving force [4] but it can lack in practical applications, where the active plastic zones originates from the crack cannot be separated from other source of plastic deformation in the system [5].

The fracture mechanics describes as continuum mechanics tool behaviour of physically long cracks. The physically (or micromechanically) small cracks are often studied experimentally [6], [7], [8]. Here has to be said, that a threshold value of a small crack is an open issue [9] new

method to assess a crack initiation and crack growth of a small crack are in the development [10], [11], [12].

According to a literature survey, The configurational force concept is able to describe physically appropriate crack driving force for arbitrary (quasi-static) loading and yielding conditions but has drawback in some practical applications [5].

The most work was done as part of the PhD. thesis [13]. Unless stated other, the figures are taken from [13] without reference.

2. Crack driving force

According to [1] the crack with initial length a_0 in a loaded body will be extended if the “generalized crack driving force” D_{gen} is equal or larger than a “generalized crack growth resistance”

$$D_{gen} \geq R_{gen}. \quad (1)$$

The crack driving force is generally a loading parameter for the crack that tries to elongate the crack. The crack driving force comes from the work of the applied forces and (or) from the stored strain energy in the body. The crack growth resistance is a function of the material and impedes the crack extension. The fracture toughness is a material property and is measured by a fracture mechanics test where a sample with a sharp (pre-fatigued) crack with the initial length a_0 is loaded. In the test are measured the load point displacement v , the load F and the crack growth extension Δa . The crack driving force increases with loading and if $D_{gen} = R_{gen}$ crack extension occurs. The crack growth toughness $R_{gen}(\Delta a)$ is obtained in a similar way from an equilibrium $D_{gen} = R_{gen}$.

The crack growth resistance is a constant for linear elastic material behaviour. Then LEFM can be used. LEFM can be applied also in the case when the plastic zone r_{pl} is

SELECTION OF THE CRACK DRIVING FORCE CONCEPT IN CONTEXT OF LINEAR-ELASTIC AND ELASTIC-PLASTIC FRACTURE MECHANICS

Michal Kráčalík

considerably smaller than the crack length a and the sample length b . That condition is called small-scale yielding (ssy) [1], see Figure 1:

$$a, b \gg r_{pl}. \quad (2)$$

If large-scale (lsy) or general yielding conditions prevail (gy) E-PFM must be used.

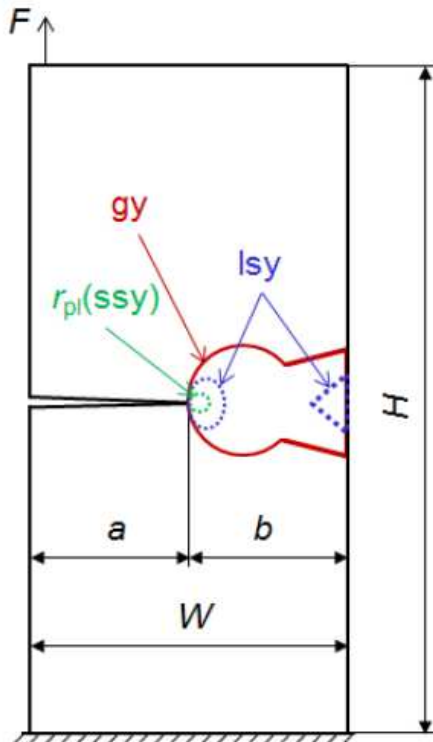


Figure 1 The loaded body with a crack of length a . The yielding conditions are distinguished by colours: green denotes small-scale yielding, blue large-scale yielding and red general scale yielding.

2.1. Crack driving force in LEFM

The two following approaches are strictly restricted to LEFM and the ssy regime resp. – elastic energy release rate G and stress intensity factor K .

2.1.1. The elastic energy release rate

The elastic energy release rate concept is useful for hard metals, composites with metal and ceramic matrix, hard strength metals and for materials where the plastic zone is negligible (LEFM or ssy regime) and is not changing during the crack growth. Then the crack growth resistance is equal twice specific surface energy γ_s and a specific plastic work for building the fracture surface γ_{pl} [1]:

$$R_{frs} = 2\gamma_{frs} = 2(\gamma_s + \gamma_{pl}). \quad (3)$$

The elastic energy release rate is expressed for a small interior crack of length $2a$. Loaded by the remote stresses σ_{appl} in an infinite plate as [1]:

$$G = \frac{\pi\sigma_{appl}^2 a}{E'}, \quad (4)$$

where E' for plane strain is expressed as $E' = E/(1 - \nu)$ and for plane stress $E' = E$ with E as the Young modulus and ν as the Poisson number. The critical length for a given applied stress can be calculated as:

$$a_{crit} = \frac{2\gamma_{frs} E'}{\pi\sigma_{appl}^2}. \quad (5)$$

Thus, the critical applied stress for a given crack length is:

$$\sigma_{appl,crit} = \sqrt{\frac{2\gamma_{frs} E'}{\pi a}}. \quad (6)$$

2.1.2. The stress intensity factor

The stress intensity factor K is dependent generally on the applied load (stress), the geometry of the body and the crack length a [1]:

$$K = \sigma_{appl} \sqrt{\pi a} f_k \left(\frac{a}{W}, \frac{H}{W} \right), \quad (7)$$

where $\sigma_{appl} = F/(BW)$ is the nominal stress, B is the thickness, W is the width and H is the height of the sample, see Figure 1. The crack starts to grow analogously to equation (1) if the stress intensity factor (applied stress tip field) K is equal or higher than the critical stress intensity factor K_c . Assuming plane strain state condition, the thickness of sample must be substantial larger than the radius of the plastic zone and is according to [1] expressed as (see also equation (2)):

$$a, b, B \geq 2.5 \frac{K_c^2}{\sigma_{YS}^2}, \quad (8)$$

where σ_{YS} is the yield strength of the material.

The stress intensity factor range ΔK can be in many cases related to the crack extension per load cycle of a fatigue crack da/dN but again LEFM (ssy) must be applicable [2].

2.2. Crack driving force in E-PFM

2.2.1. The crack tip opening displacement (CTOD)

CTOD characterizes the intensity of the near-tip field also in cases where LEFM is not applicable [1]. The crack grows in analogy to equation (1) if CTOD δ is equal or higher than critical CTOD δ_c . The δ_c is taken at $\Delta a = 0.2mm$. To characterize the intensity of the near-tip field

SELECTION OF THE CRACK DRIVING FORCE CONCEPT IN CONTEXT OF LINEAR-ELASTIC AND ELASTIC-PLASTIC FRACTURE MECHANICS

Michal Kráčalík

via CTOD the crack and the sample length as well as the sample thickness must be much larger than δ_c [1]:

$$a, b, B \geq \delta_c. \quad (9)$$

The cyclic crack tip opening displacement, $\Delta\delta_t = \delta_{t,max} - \delta_{t,min}$, can be expressed in form of the stress intensity factor range ΔK according to [2] as:

$$\Delta\delta_t = \alpha \frac{(\Delta K)^2}{2E\sigma_y}, \quad (10)$$

where α is a constant and is approximately equal to 0.5 for plane stress and 0.5 for plane strain, σ_y is the yield stress.

2.2.2. The J-integral

The J-integral measures the difference of the potential energy of two identical non-linear elastic bodies with

different crack lengths, see Figure 2. Following [14], assumed is a homogeneous body with non-linear elastic material properties. Plane strain condition and no volume forces are imposed on the body. The crack lies in x-direction in the body. For those assumptions the J-integral is [1], [14]:

$$J = \int_{\Gamma} \left(\Phi dy - T_i \frac{\partial u_i}{\partial x} ds \right) = -\frac{1}{B} \frac{dP}{da}, \quad (11)$$

where Γ is the curve around the crack tip, ds is the element on the curve Γ , u_i is the displacement vector, T_i is the traction vector, P is the potential energy of the body. The deformation energy in the body is defined as [1], [14]:

$$\Phi = \int_0^{\varepsilon_{ij}} \sigma_{ij} d\varepsilon_{ij}. \quad (12)$$

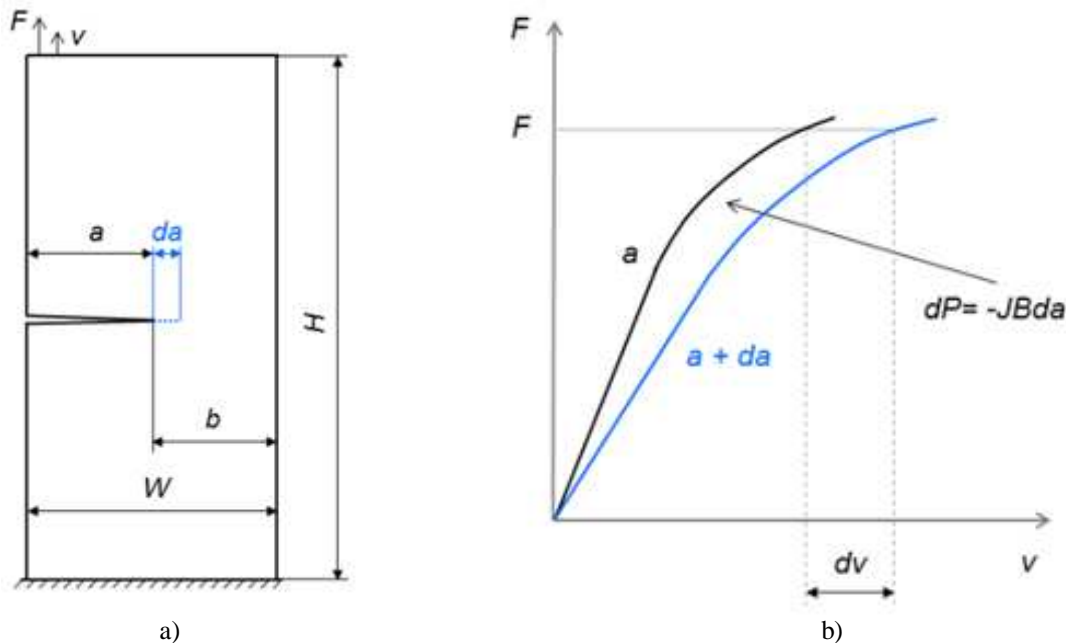


Figure 2 Non-linear elastic body with the crack of two lengths (a). The J-integral is measure of a difference in the potential energy (b).

Similarly to the previous methods, crack grows occurs if $J \geq J_c$. For the J-concept to be valid J_c requires much less strict criteria have to be satisfied to the restrictions of the K or the CTOD concept, see equations (8, 9) and compare with equation (13), [1]:

$$B \geq l_{pz}, \quad (13)$$

where l_{pz} is the length of the process zone. l_{pz} is proportional to CTOD, $l_{pz} \approx (2 \div 3)\delta$. Thus this method is useful for a correct determination of the crack growth resistance J_c of a low strength material. The required

sample size is in order of magnitude smaller than what is necessary for a correct determination of K_c .

Hutchinson, Rice and Rosengren showed that J characterizes the intensity of the crack tip field for elastic-plastic materials (so-called HRR field). Deformation plasticity and power-law hardening are assumed. Then the strain energy density near the crack tip follows the relationship $\Phi \sim J/r$ and the stress and strain components are given by [1]:

$$\sigma_{ij} = \sigma_0 \left(\frac{EJ}{\alpha_{RO}\sigma_0^2 l_{NR}} \right)^{1/(N+1)} \tilde{\sigma}_{ij}(N, \theta), \quad (14)$$

SELECTION OF THE CRACK DRIVING FORCE CONCEPT IN CONTEXT OF LINEAR-ELASTIC AND ELASTIC-PLASTIC FRACTURE MECHANICS

Michal Kráčalík

$$\varepsilon_{ij} = \frac{\alpha_{RO}\sigma_0}{E} \left(\frac{EJ}{\alpha_{RO}\sigma_0^2 I_N r} \right)^{N/(N+1)} \tilde{\varepsilon}_{ij}(N, \theta), \quad (15)$$

where the stresses and strains are dependent on the polar coordinates (r, θ) with respect to the crack tip, α_{RO} is a dimensionless constant, σ_0 is a reference stress and is equal to the yield strength for a small α_{RO} , ε_0 is a reference strain ($\varepsilon_0 = \sigma_0/E$), N is a hardening parameter with value of 1 for a linear elastic material description and ∞ for an ideally plastic material description. The parameter I_N and the functions $\tilde{\sigma}_{ij}, \tilde{\varepsilon}_{ij}$ are tabulated as a function of N .

The conventional J-integral is not appropriate for non-proportional cyclic loading and does not characterize the real crack driving force for a crack in an elastic-plastic material [4]. The experimental cyclic J-integral ΔJ^{exp} was

proposed as a parameter characterizing the crack growth rate da/dN of fatigue cracks for cases where ΔK is not applicable anymore.

2.2.3. The configurational force concept

The configurational force concept is based on a thermodynamic framework and Eshelby's energy momentum tensor. The concept is able to account for an incremental theory of plasticity. Another concept, the previously mentioned J-integral is developed based on deformation theory of plasticity. It has been shown in [2] [15] [16] that a calculated crack driving force based on the deformation theory leads to incorrect results in cyclic loading. The principle difference between the two theories of plasticity is shown in Figure. 3.

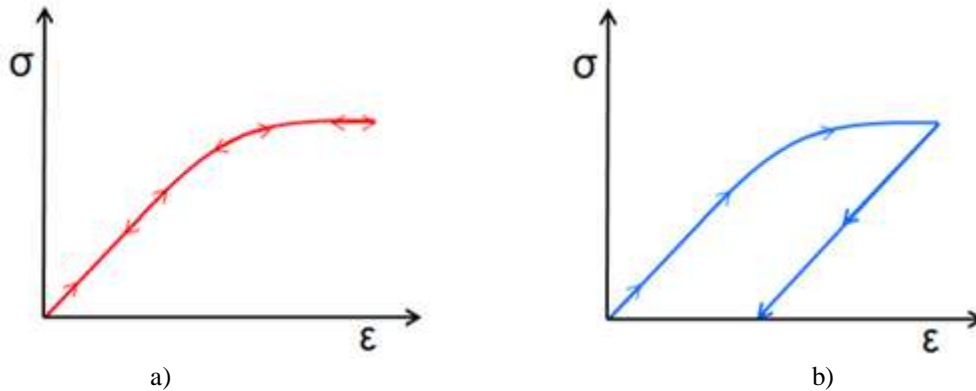


Figure 3 The stress-strain behaviour of the material described by deformation theory of plasticity is (a); the behaviour using incremental theory of plasticity (b).

The plastic strain in the deformation theory of plasticity is described as a function of equivalent strain $\varepsilon_p \approx \sigma_{eq}$, which is in effect a description for a non-linear elastic material, see Figure 3a and [1]. The incremental theory of plasticity describes an increment of plastic strain as a function of the equivalent stress: $d\varepsilon_p \approx \sigma_{eq}$, see Figure 3b and [1]. The two descriptions of the plastic strain results in different energy considerations as can be seen in the area below the stress-strain curve, see Figure 4 and [15]. The whole strain energy density Φ below the stress-strain curve can be divided into an elastic part Φ_{el} and a plastic part Φ_{pl} . Then the configurational body force vector can be

written for the deformation theory of plasticity (non-linear elastic material description) as:

$$f^{nel} = -\nabla(\Phi I - F^T S) \quad (16)$$

and for the incremental theory of plasticity as:

$$f^{ep} = -\nabla(\Phi_{el} I - F^T S), \quad (17)$$

where I is the unit tensor, F^T is the transposed deformation gradient tensor, S is the first Piola-Kirchhoff stress tensor.

SELECTION OF THE CRACK DRIVING FORCE CONCEPT IN CONTEXT OF LINEAR-ELASTIC AND ELASTIC-PLASTIC FRACTURE MECHANICS

Michal Kráčalík

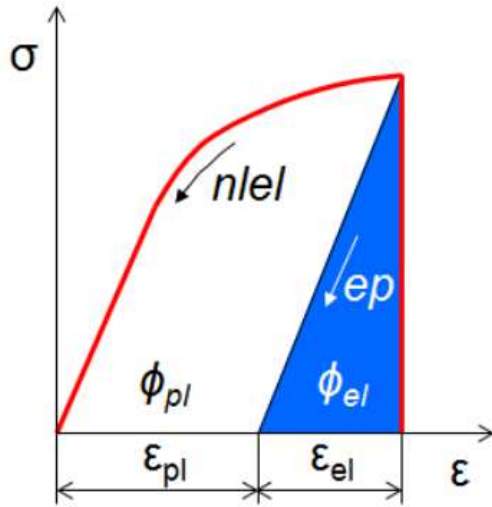


Figure 4 The energy consideration below the stress-strain curve. The whole area below the red curve represents the energy consideration according to the deformation theory of plasticity. The blue part represents the energy consideration of the incremental theory of plasticity. The plastic part of the strain energy density (white) is consumed during plastic deformation and only the elastic part is available for driving the crack.

The thermodynamic crack driving force for elastic-plastic materials along an arbitrary integration contour Γ_r (here shown for a crack driving force which originates from the crack tip contour $\Gamma_r \rightarrow 0 \Rightarrow J_{tip}^{ep}$) is expressed as [15]:

$$J_{tip_i}^{ep} = e_i \int_{\Gamma_r} (\phi_{el} I - F^T S) m dl, \quad (18)$$

where e_i is the unit vector related to the chosen direction of the local coordinate system of the crack, see Figure 5; m is the unit normal vector on the integration contour Γ_r and dl is the infinitesimal small length on the circumference Γ_r .

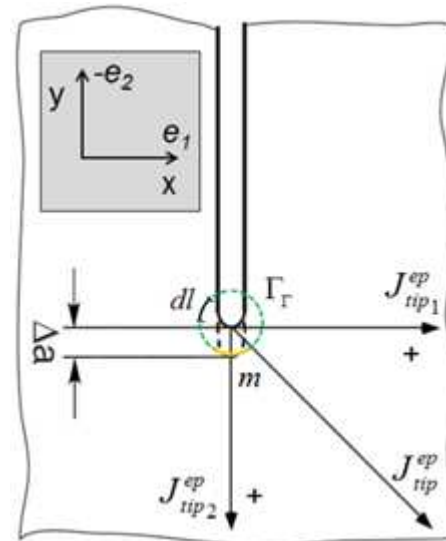


Figure 5 Sketch of the crack driving force vector which originates from the crack tip. The unit vectors are chosen in order to plot the crack driving force as function of the crack modes. Δa represents a virtual crack growth extension only when the crack driving force related to the crack Mode I $J_{tip_2}^{ep}$ supports crack growth.

3. Evaluation of the crack driving force approaches

The evaluated fracture mechanics (crack driving force) approaches are summarised in Table 1. The energy release rate and the stress intensity factor are restricted to LEFM or SSY, while other approaches can be used in E-PFM. The configurational force concept is not restricted for monotonic loading and can be used for arbitrary (quasi-static) loading and yielding conditions (denotes as cyclic plastic loading in the Table 1).

Table 1 Regime of the validity of various fracture mechanics approaches

	Loading Parameter for the Crack	Regime of Validity
Linear elasticity	Elastic energy release rate G (J/m^2)	<ul style="list-style-type: none"> linear elastic fracture mechanics (LEFM) small-scale yielding
	Stress intensity factor K ($Nm^{-3/2}$)	<ul style="list-style-type: none"> LEFM small-scale yielding
General usage	Crack tip opening displacement (CTOD) δ (mm)	<ul style="list-style-type: none"> small-scale yielding large-scale yielding general yielding
	J-integral J (J/m^2)	<ul style="list-style-type: none"> LEFM small-scale yielding large-scale yielding general yielding
	No cyclic plastic loading	<ul style="list-style-type: none"> LEFM small-scale yielding large-scale yielding general yielding
	Configurational force concept J^{ep} (J/m^2)	<ul style="list-style-type: none"> LEFM small-scale yielding large-scale yielding general yielding
	Cyclic plastic loading	<ul style="list-style-type: none"> small-scale yielding large-scale yielding general yielding

SELECTION OF THE CRACK DRIVING FORCE CONCEPT IN CONTEXT OF LINEAR-ELASTIC AND ELASTIC-PLASTIC FRACTURE MECHANICS

Michal Kráčalík

Conclusion

Crack driving force concepts are described and evaluated in regard to LEFM and E-PFM in the paper. The regime of their validity are summarised in the table. The configurational force concept is able to handle with arbitrary (quasi-static) loading and yielding conditions. In the introduction is discussed limitation of the concept in the practical applications.

References

- [1] KOLEDNIK, O.: *Fracture Mechanics*, Wiley Encyclopedia of Composites.: American Cancer Society, pp. 1-16, 2012.
- [2] OCHENSBERGER, W., KOLEDNIK, O.: A new basis for the application of the J-integral for cyclically loaded cracks in elastic-plastic materials, *International Journal of Fracture*, Vol. 189, pp. 77-101, 2014.
- [3] FLOROS, D., EKBERG, A., RUNESSON, K.: A numerical investigation of elastoplastic deformation of cracks in tubular specimens subjected to combined torsional and axial loading, *International Journal of Fatigue*, Vol. 91, pp. 171-182, 2016.
- [4] OCHENSBERGER, W., KOLEDNIK, O.: Physically appropriate characterization of fatigue crack propagation rate in elastic-plastic materials using the J-integral concept, *International Journal of Fracture*, Vol. 192, pp. 25-45, 2015.
- [5] DAVES, W., KRÁČALÍK, M.: Cracks Loaded by Rolling Contact - Influence of Plasticity around the Crack, *Materials Structure & Micromechanics of Fracture VIII*, Vol. 258, jan., pp. 221-224, 2017.
- [6] HELGESEN, T., TJERNÆS, A., HEIBERG, G., HEIER, E.: Failure investigation and condition assessment using field metallography, *Engineering Failure Analysis*, Vol. 12, pp. 974-985, 2005.
- [7] POLÁK, J., MAN, J.: Experimental evidence and physical models of fatigue crack initiation, *International Journal of Fatigue*, Vol. 91, pp. 294-303, 2016.
- [8] YAHUI LIU, MAODONG KANG, YUN WU, MENG MENG WANG, HAIYAN GAO, JUN WANG.: Effects of microporosity and precipitates on the cracking behavior in polycrystalline superalloy Inconel 718, *Materials Characterization*, Vol. 132, pp. 175-186, 2017.
- [9] ZERBST, U., VORMWALD, M., PIPPAN, R., GÄNSER, H.P., SARRAZIN-BAUDOUX, Ch., MADIA, M.: About the fatigue crack propagation threshold of metals as a design criterion - A review, *Engineering Fracture Mechanics*, Vol. 153, pp. 190-243, 2016.
- [10] MAIERHOFER, J., PIPPAN, R., GÄNSER, H.-P.: Modified NASGRO equation for physically short cracks, *International Journal of Fatigue*, Vol. 59, pp. 200-207, 2014.
- [11] KRÁČALÍK, M., DAVES, W.: Crack growth assessment in rolling/sliding contact, Proceedings of the EUROMECH Colloquium 578 in Rolling Contact Mechanics for Multibody System Dynamics, J. Ambrosio, W. Schielen, and J. Pombo, Eds.: IDMEC, p. 54., 2017.
- [12] TRUMMER, G., MARTE, C., DIETMAIER, P., SOMMITSCH, C., SIX, K.: Modeling surface rolling contact fatigue crack initiation taking severe plastic shear deformation into account, *Wear*, Vol. 352-353, pp. 136-145, 2016.
- [13] KRÁČALÍK, M.: *Influence of the vehicle-track parameters on the crack growth in rails*, Dissertation thesis, 2015.
- [14] ANDERSON, Ted L., ANDERSON, T.L.: *Fracture Mechanics: Fundamentals and Applications*, 3rd ed., CRC Press, 2005.
- [15] KOLEDNIK, O., SCHÖNGRUNDNER, R., FISCHER, F.D.: A new view on J-integrals in elastic-plastic materials, *International Journal of Fracture*, Vol. 187, pp. 77-107, May 2014. doi:10.1007/s10704-013-9920-6
- [16] KRÁČALÍK, M., DAVES, W., ANTRETTER, T.: Calculation of crack driving forces of surface cracks subjected to rolling/sliding contact, *Engineering Fracture Mechanics*, Vol. 152, pp. 10-25, 2016.

Review process

Single-blind peer review process.

SNAKE-LIKE ROBOTS

Ivan Virgala; Ľubica Miková; Michal Kelemen; Darina Hroncová

doi:10.22306/am.v3i4.43

Received: 26 Sep. 2018

Accepted: 16 Oct. 2018

SNAKE-LIKE ROBOTS**Ivan Virgala**

Technical University of Kosice, Faculty of Mechanical Engineering, Letna 9, Kosice, Slovak Republic,
ivan.virgala@tuke.sk (corresponding author)

Ľubica Miková

Technical University of Kosice, Faculty of Mechanical Engineering, Letna 9, Kosice, Slovak Republic,
lubica.mikova@tuke.sk

Michal Kelemen

Technical University of Kosice, Faculty of Mechanical Engineering, Letna 9, Kosice, Slovak Republic,
michal.kelemen@tuke.sk

Darina Hroncová

Technical University of Kosice, Faculty of Mechanical Engineering, Letna 9, Kosice, Slovak Republic,
darina.hroncova@tuke.sk

Keywords: mechatronics, education, embedded systems

Abstract: The paper deals with snake-like robots. There are several types of snake-like locomotions. Biological example – snake always select the best type of locomotion in accordance with terrain. Big manoeuvrability leads many teams to develop snake-like robots. These structures have many degree of freedom and it is complicated to control them.

1 Introduction

Many ground locomotion devices often use endless rotating elements such as wheels or tracks. Endless rotating elements are the fascinating elements in machines. These elements have one big disadvantage. They are not suitable for extremely rough terrain. There is no analogy for wheels and tracks in the nature. In this time, there are a lot of applications with biologically inspired locomotion. Place for biologically inspired locomotion is mainly in cases, where we cannot use wheels or tracks. Living organisms are able to adapt to surround conditions, because of its physiological needs. Consequently, they are able to change own shape and locomotion type.

Biologically inspired snake robots are able to perform the motion in environments where other types of transport mechanisms fail. Snake robots are usually composed of many identical segments. A snake robot's body structure is self-enabling, and offers mechanical transport performance characteristics that are highly desired. However, snake robot body structures are difficult to control.

The most famous research of snake like locomotion comes from Hirose & Yoneda Lab. Their results are summarized in book [1].

They have observed four basic types of snake locomotion. Using of these locomotion types depends on environment condition and purpose of locomotion. These locomotion types can be divided into these four modes [1]:

1. serpentine locomotion
2. rectilinear locomotion
3. concertina locomotion
4. sidewinding locomotion

Serpentine locomotion is the locomotion to be seen typically in almost kinds of snake, and is a gliding mode whose characteristic is that each part of body makes similar tracks. From ancient times this has been the mode which has propelled snakes like flowing water between rocks, for instance, and has surprised humans, and of the four modes this can be thought of as the most efficient.

Rectilinear locomotion is the gliding method performed with a special configuration by large snake such as boas and vipers when approaching their prey or when gliding over a smooth surface.

Concertina locomotion is gliding method used by snakes confined to a straight path over a narrow straight line, and by snakes placed on floor surfaces, for example, which are extremely slippery. In particular, the gliding configuration on such a floor surface uses the phenomenon that theoretical terms the coefficient of the static friction is greater than the coefficient of dynamic friction. For this reason, propulsion is possible even in a very slippery environment, using this gliding mode. However, the efficiency of such propulsion is extremely low.

Sidewinding locomotion is the gliding method used by snake such as the rattle-snake which live in the desert, and which lift part of their body while gliding and propel themselves like a tumbling spiral coil. In this mode of locomotion, there is no sliding movement between the body and surface glided over, its dynamic characteristic being that the body usually contacts the ground from above. Because of this characteristic, sliding friction resistance is small, and in locomotions in environments which are not firm, such as sandy ground, the locomotive efficiency is high [1].

SNAKE-LIKE ROBOTS

Ivan Virgala; Ľubica Miková; Michal Kelemen; Darina Hroncová

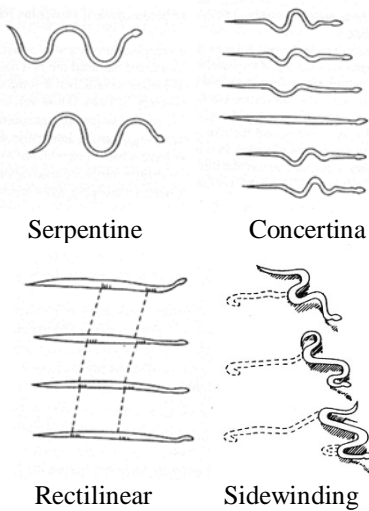


Figure 1 Snake-like locomotion modes [1]

2 Concept of the snake-like robot composed from 1DOF segments

Snake-like robot consist of many joints for obtaining of many degree of freedom to obtain high level of mobility. Many joints means many actuators and complicated controlling. For this reason, it is necessary to make decision. How many joints is necessary for robot. We have to select as least as possible.

Our robot “Hadik” consists of eight articles also called as segments joined with seven plane joints (fig. 2). Every segment has one degree of freedom (DOF). The base of the kinematic principle lies on alternating of vertical and horizontal plane joints. First article (head) and last article (tail) are designed with vertical plane joint, because of their possibility to cross any obstacles (fig. 3). Therefore, every kinematic pair is designed with one degree of freedom.

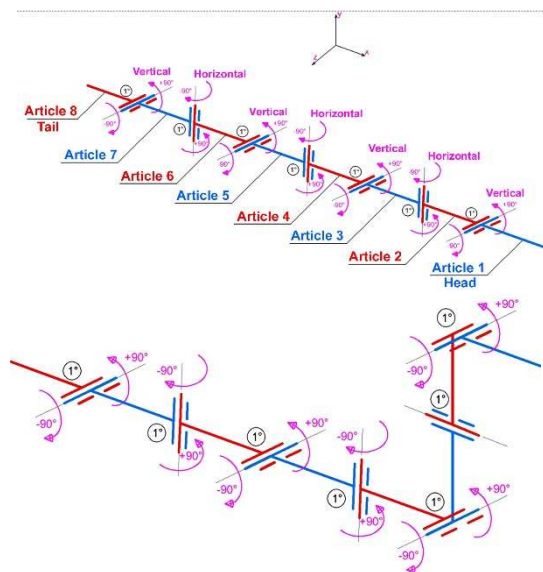


Figure 2 Structure of snake-like robot “Hadik”

Every article has one degree of freedom in regard to neighbour robot article. These plane joints are driven with actuators. As actuator is chosen position servomechanism. General problem for design of locomotion algorithm is timing of sequence. Time of every joint rotation is dependent on its loading and position. Therefore, microcontroller needs information about actual angular position of every joint. Ideal solution is to use information from internal potentiometer as feedback for our microcontroller.

The article of the robot consists of 13 parts. Symmetry and precision of every part has been very important requirement. It has been needed for obtaining of stabile locomotion.

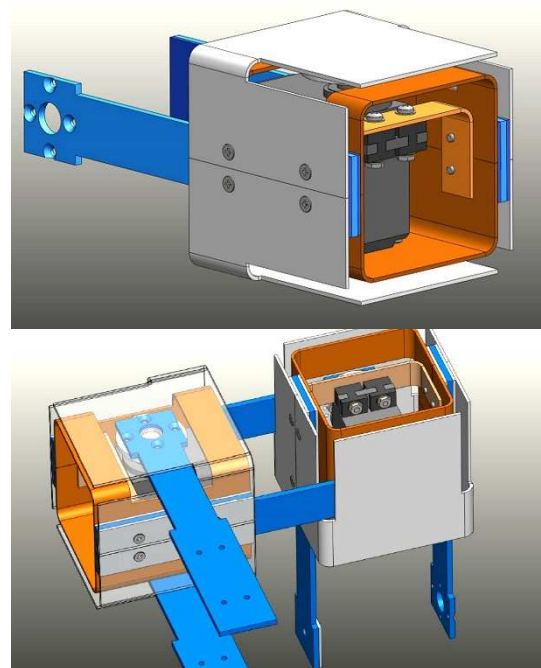
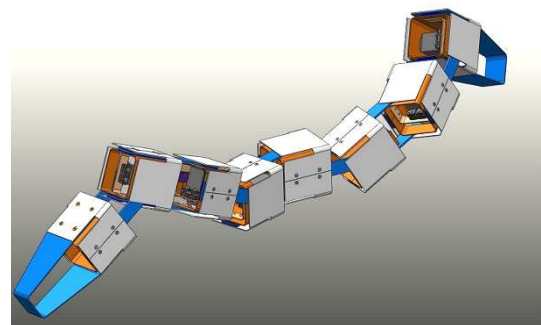


Figure 3 Article (segment) of the snake-like robot

3D model has been created for verification of functionality and possible collisions between parts in locomotion. Realisation of the robot brought several problems. It has been necessary to solve technology process, precision of bending, placement of wires etc. (fig. 4).



SNAKE-LIKE ROBOTS

Ivan Virgala; Ľubica Miková; Michal Kelemen; Darina Hroncová

Figure 4 3D model of the snake-like robot

Realisation of the snake-like robot “Hadik” is shown on figure 5.



Figure 5 Realisation of the snake-like robot “Hadik”

3 Concept of the snake-like robot composed from 2DOF segments

Concept of snake-like robot “Locosnake” consists of segments with 2 degree of freedom (DOF). Figure 6 shows the kinematic structure of it.

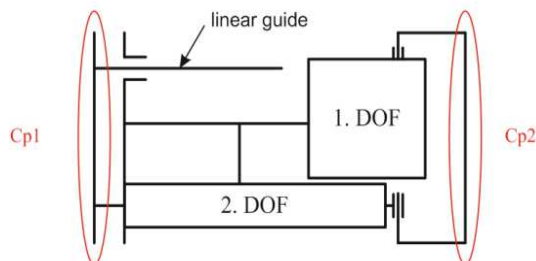


Figure 6 Concept of 2DOF segment for snake-like robot “Locosnake”

LocoSnake is a unique kinematic structure not previously utilized. Each segment of the snake robot possesses two degrees of freedom. Along one degree of freedom, a segment may rotate $\pm 90^\circ$ (fig. 7). Along the other, a segment may effect a linear translation up to 50mm (fig. 8). Each segment end is equipped with a clutch which enables the connection of other parts, signal cables, and provides power source cable transportation, see Figure 6.

The kinematic structure of the snake robot was designed using SolidWorks software, see Figure 2 and 3 for models. It was necessary to specify dimensional requirements to ensure the accuracy of the model’s configuration. The dimensions of the model’s action parts were most important.



Figure 7 Rotation in segment for snake-like robot “Locosnake”

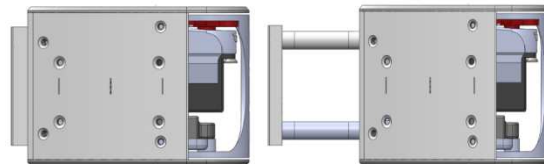


Figure 8 Linear stroke in segment for snake-like robot “Locosnake”

LocoSnake was constructed from parts made by a 3D printer. One link of Lo-coSnake weighs 250 g and has a maximum length of 131 mm, width of 80,2 mm, and height of 47 mm. Figure 9 shows the realisation of snake-like robot “Locosnake”.

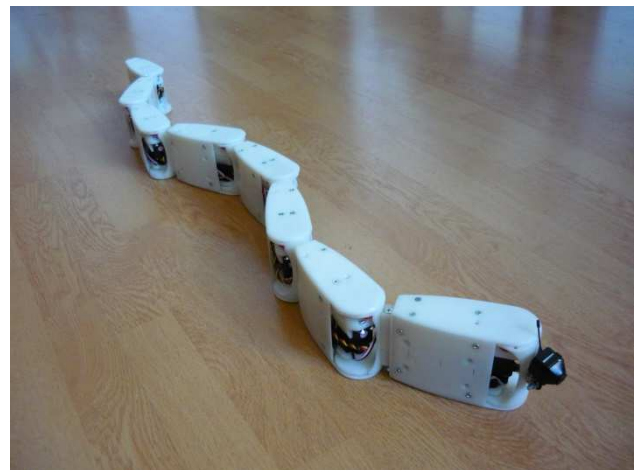


Figure 9 Realisation of snake-like robot “Locosnake”

4 Conclusion

Locomotion is basic of the live of living organisms. They need locomotion for food finding, for avoiding from enemy or another dangerous. Ways of locomotion are very often as inspiration for design of various locomotion devices [2-21].

Snake robots possess the ability to work within a broad range of applications where conventional mechanisms ineffective. These robots, inspired by the nature, provide potential solutions to designers and researches, and they introduce numerous undetermined questions and problems. Pipe inspection is an application snake robots are well suited to, and this area of application has not yet been investigated in detail.

SNAKE-LIKE ROBOTS

Ivan Virgala; Ľubica Miková; Michal Kelemen; Darina Hroncová

Acknowledgement

The authors would like to thank to Slovak Grant Agency – project KEGA 018TUKE-4/2018, VEGA 1/0389/18, VEGA 1/0872/16 and FGV/2016 supported by Faculty of Mech. Eng. at Technical University of Kosice.

References

- [1] HIROSE, S.: Biologically Inspired Robots. Snake-like locomotors and manipulators. Oxford University Press. New York, 1993. ISBN 0 19 856261 6
- [2] ACAR, M., and PARKIN, R.M.: Engineering Education for Mechatronics, *IEEE Trans. on Industrial Electronics*, vol. 43, no. 1, pp. 106-112, Feb. 1996.
- [3] CASTLES, R. T., ZEPHIRIN, T., LOHANI, V. K., KACHROO, P.: Design and Implementation of a Mechatronics Learning Module in a Large First-Semester Engineering Course, *IEEE Trans. on Education*, vol. 53, no. 3, pp. 445-454, Aug. 2010.
- [4] OSTOJIC, G., STANKOVSKI, S., TARJAN, L., SENK, I. and JOVANOVIĆ, V.: Development and Implementation of Didactic Sets in Mechatronics and Industrial Engineering Courses, *Int. J. of Eng. Education*, vol. 26, no. 1, Tempus publications, 2010.
- [5] BRADLEY, D.: What is Mechatronics and Why Teach It?, *Int. J. of Electrical Eng. Education*, 41, (2004), pp. 275-291, 2004
- [6] BRADLEY, D.: Mechatronics - More questions than answers, *Mechatronics*, vol. 20, no. 8, Special Issue on Theories and Methodologies for Mechatronics Design, pp. 827-841, Dec. 2010.
- [7] VITKO, A., JURIŠICA, L., BABINEC, A., DUCHOŇ, F., KLUČIK, M.: *Some Didactic Problems of Teaching Robotics*, Proceedings of the 1st International Conference Robotics in Education 2010. Bratislava, 16.-17. 9. 2010, Bratislava, Slovak University of Technology in Bratislava, ISBN 978-80-227-3353-3, pp. 27-30, 2010.
- [8] KONIAR, D., HARGAS, L., SIMONOVA, A. et al.: *Virtual Instrumentation for Visual Inspection in Mechatronic Applications*, 6th Conference on Modelling of Mechanical and Mechatronic Systems (MMaMS) Location: Vysoke Tatry, SLOVAKIA Date: NOV 25-27, 2014.
- [9] van BEEK, T. J., ERDENA M. S., TOMIYAMAA, T.: Modular design of mechatronic systems with function modeling, *Mechatronics*, vol. 20, no. 8, pp. 850-863, Dec. 2010.
- [10] WANG, Y., YUA, Y., XIEA, Ch., WANGA, H., FENG, X.: Mechatronics education at CDHAW of Tongji University: Laboratory guidelines, framework, implementations and improvements, *Mechatronics*, vol. 19, no. 8, pp. 1346–1352, Dec. 2009.
- [11] KELEMEN, M., KELEMENOVÁ T. and JEZŇ, J.: Four legged robot with feedback control of legs motion. In: *Bulletin of Applied Mechanics*. Vol. 4, no. 16 (2008), p. 115-118. - ISSN 1801-1217.
- [12] VIRGALA, I., VACKOVÁ, M., KELEMEN, M.: Two-legs walking robot "Wirgil". In: *Medical and treatment*. Vol. 40, no. 2 (2010), p. 32-35. - ISSN 0301-5491.
- [13] MIKOVÁ, Ľ., KELEMEN, M., KELEMENOVÁ, T.: Four wheeled inspection robot with differential controlling of wheels. In: *Acta Mechanica Slovaca*. Vol. 12, č. 3-B (2008), s. 548-558. - ISSN 1335-2393.
- [14] DUCHOŇ, F., HUBINSKÝ, P., HANZEL, J., BABINEC, A., TÖLGYESSY, M.: Intelligent Vehicles as the Robotic Applications, *Procedia Engineering*, Volume 48, 2012, Pages 105–114. 2012.
- [15] KONIAR, D., HARGAŠ, L., ŠTOFAN, S.: Segmentation of Motion Regions for Biomechanical Systems, *Procedia Engineering*, Volume 48, 2012, Pages 304–311. 2012.
- [16] BOŽEK, P., CHMELÍKOVÁ, G.: *Virtual Technology Utilization in Teaching*, Conference ICL2011, September 21 -23, 2011 Piešťany, Slovakia, pp- 409-413. 2011.
- [17] TURYGIN, Y., BOŽEK, P.: Mechatronic systems maintenance and repair management system. *Transfer of innovations*, 26/2013. pp. 3-5. 2013.
- [18] HARGAŠ, L., HRIANKA, M., KONIAR, D., IZÁK, P.: *Quality Assessment SMT Technology by Virtual Instrumentation*. Applied Electronics 2007, 2007.
- [19] SPANIKOVA, G., SPANIK, P., FRIVALDSKY, M. et al.: Electric model of liver tissue for investigation of electrosurgical impacts, *Electrical Engineering*, Volume: 99, Issue: 4, pp. 1185-1194.
- [20] KARAVAEV, Y. L., KILIN, A. A.: Nonholonomic dynamics and control of a spherical robot with an internal omniwheel platform: Theory and experiments, *Proceedings of the Steklov Institute of Mathematics*, Volume 295, Issue 1, 1 November 2016, Pages 158-167.
- [21] Kuric, I., Bulej, V., Saga, M., Pokorný, P., *Development of simulation software for mobile robot path planning within multilayer map system based on metric and topological maps*, International Journal of Advanced Robotic Systems, Volume: 14 Issue: 6, pp. 1-14.

Review process

Single-blind peer review process.

DESIGN OF BODY WHEEL SHAPE TO IMPROVE TEETH STIFFNESS FOR GEARBOX OF MECHATRONIC SYSTEMS

Silvia Medvecká-Beňová

Technical University of Kosice, Faculty of Mechanical Engineering, Letna 9, Kosice, Slovak Republic, EU, silvia.medveckea@tuke.sk (corresponding author)

Peter Frankovský

Technical University of Kosice, Faculty of Mechanical Engineering, Letna 9, Kosice, Slovak Republic, EU, peter.frankovsky@tuke.sk

Keywords: mechatronics, gearbox, teeth deformation, spur gear, finite element method

Abstract: The most important component of your drive systems of mechatronic units are geared systems. Prospective application of highly accurate transfers it can be examined by the need to adapt to our own design, size and the minimum weight transfer. It is anticipated construction material so flow density, high stiffness, reliability, positioning, control. Increasing performance and improving load machines with gear unit leads to increase the technical level of machines. This process is often at the cost of degradation of the environment. One of the factors that aggravate environmental is a noise. Periodic changes the stiffness of the tooth during meshing in gear drives mainly affects of the noise in the transfer. The work is devoted to the analysis of influence of the body wheel shape on the tooth stiffness. The problem is solved for spur gears. As the basis for calculating the tooth stiffness are results of teeth deformation. The teeth deformation has be solution problem by finite element method.

1 Introduction

Gear wheels became a symbol of engineering. They are the basic element, through which transmission and transformation of mechanical power and movement are implemented in machines [1-3]. They are one of the most complicated mechanical components from the theoretical, construction and production viewpoint. The machines and machineries with gear transmission are very popular and draw sufficient attention. The weight reduction of the construction machines and engine plants as well as increasing of their efficiency and productivity, are all part of the important task in the area of the construction, technology and research workers must accomplish them [4].

2 Definition of tooth stiffness

Deformation of teeth is usually expressed quantitatively as a teeth stiffness during by gear mesh [5]. In general, stiffness defined as the ratio of load to deformation. The stiffness of the tooth is defined as the force per unit width, which is necessary for the deformation about $1\mu\text{m}$ [6-8]. Theoretical determination of teeth deformation of involute gears is difficult, because the tooth profile is consists of involute and smooth fillet. The previous experimental procedures were based on the static deformation measurements gearing loaded constant force, or seismic measurement deviations as you turn. But it requires the construction of a suitable model and use of appropriate machinery, given the limited value of deformation quality measurement technology. The matter in question is thus preferable to solve finite element, which

is one of the most widely used numerical methods. The tooth deformation of spur gears is not constant for all examined teeth of gears. The deformation of the teeth depends on the shape of the teeth, thus the basic parameters of the gearing and on the shape and construction of the body wheel and the wheel load.

As has been said, the teeth of the gear wheels are deformed due to load. This is the cause of some negative but also positive consequences. Therefore, the knowledge of the deformation properties of the teeth is very important [9]. The theoretical determination of the teeth deformation is difficult due to the complex shape of the gear teeth. In recent years, the question of teeth deformation has been solved using modern methods of calculation, for example by a finite element method. The finite element method is used to determine the teeth deformation [11-12]. We will focus on the value of the total deformation in the direction of action forces (Figure 3). On the basis of the teeth deformation, the stiffness of the teeth is calculated. In general the teeth stiffness c is defined by equation (1):

$$c = \frac{w}{\delta} \quad (1)$$

where c – tooth stiffness [N/mm.μm],
 w – load across the width of the teeth [N/mm],
 δ – tooth deformation [μm].

The teeth stiffness values are the basis for assessing the suitability of design of the wheels of mechatronic system in this paper.

DESIGN OF BODY WHEEL SHAPE TO IMPROVE TEETH STIFFNESS FOR GEARBOX OF MECHATRONIC SYSTEMS

Silvia Medvecká-Beňová; Peter Frankovský

3 Design of various types of gear wheels

Achieving the smallest weight of the spur gear wheel is the designer's effort in designing the shape of a large gear wheel body. However, the reduction of the load-bearing cross-sections is usually limited by the requirement for sufficient stiffness of the bodies. In the case of gears it is gear mesh stiffness.

Large-dimensional gear wheels can be made as monolithic one, the most commonly are a forged and cast gear wheels. Spur gears with a diameter of 200 to 500mm are produce of forged blanks most commonly. Larger spur gears with a diameter of over 500mm may be produce as a cast blanks. But striving to improve the design of the gears, aimed at reducing the dimensions and weight, has be led to the used of gears with thin-walled gear rim and with thin gear rim. Figure 1 shows an example of design a forged and cast body of spur gear wheel.

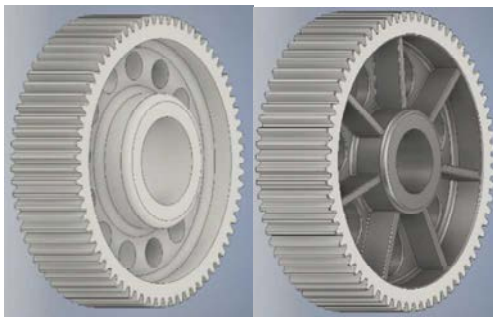


Figure 1 Design of body gear wheel

The wheel rim thickness (s_R) and wheel web thickness (b_s) (in Figure 2) are important parameters which influence of weight of gear wheel. In the next section, the paper will focus on the influence of wheel rim and web parameters on the tooth stiffness of spur gears.

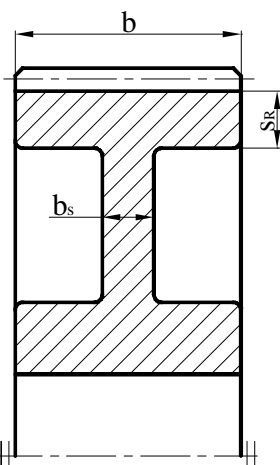


Figure 2 Design of gear wheel

4 Influence of the shape of body gears wheel on the tooth stiffness

Achieving The impact of the rim thickness (value s_R in Figure 2) on the deformation and stiffness of the tooth will be determined on the spur gear with a number of teeth of $z=61$ and a module $m_n=4\text{mm}$ and a tooth width $b=80\text{mm}$.

Will be examined the tooth stiffness under load $F=5000\text{ N}$, if the if the force is applied to the head of the tooth (the largest bend) according to Figure 3.

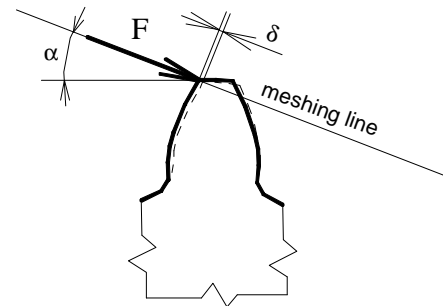


Figure 3 Deformation of tooth

Will be examined the tooth stiffness under load $F=5000\text{ N}$, if the if the force is applied to the head of the tooth (the largest bend) according to Figure 3. The thickness of the wheel rim is changed from the value $s_R=1.75m_n$ ($2.5m_n$, $3.5m_n$, $5m_n$, $8m_n$ and full wheel) to the full body of the wheel. These results are determined by the finite element method and are processed in the graph in Figure 4.

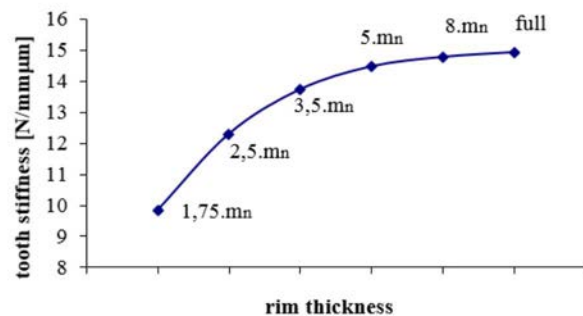


Figure 4 Influence of wheel rim on the tooth stiffness

As the results show, decreasing the thickness of the rim wheel is increases the tooth deformation and the tooth stiffness is decreases. The minimum permissible thickness of the wheel rim according to [10] is $s_R = 3.5m_n$, where m_n is a modul of the gear wheel. Thickness of wheel rim less than value $3.5 m_n$ has more affects to the tooth deformation and stiffness. Thickness of wheel rim bigger than value $3.5 m_n$ has smaller affects to the teeth deformation and stiffness, as show in the Figure 4.

The impact of the rub thickness (value b_s -Figure 2) on the tooth stiffness will be determined on the spur gear with a number of teeth of $z=61$ and a module $m_n=4\text{mm}$ and a

DESIGN OF BODY WHEEL SHAPE TO IMPROVE TEETH STIFFNESS FOR GEARBOX OF MECHATRONIC SYSTEMS

Silvia Medvecká-Beňová; Peter Frankovský

tooth width $b=80\text{mm}$, the value of wheel rim is $s_R=22\text{mm}$. The web is located at the center of the gear wheel width and its thickness will change from 10 mm to the 80 mm, when it is a full gear wheel without a web. The force is applied to the head of the tooth (the largest bend) according to Figure 3 and the value of load across the width of the tooth is a $w=40\text{N/mm}$.

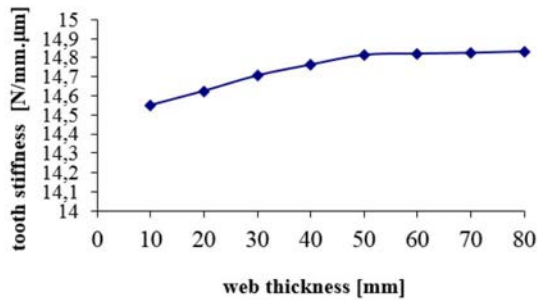


Figure 5 Influence of wheel web on the tooth stiffness

The tooth deformation is reduced and the tooth stiffness is expanded, due to the increase in the thickness of the wheel web located at the center of the gearing width, it is show in Figure 5. This change in tooth deformation and tooth stiffness is more pronounced to the first half of gearing width.

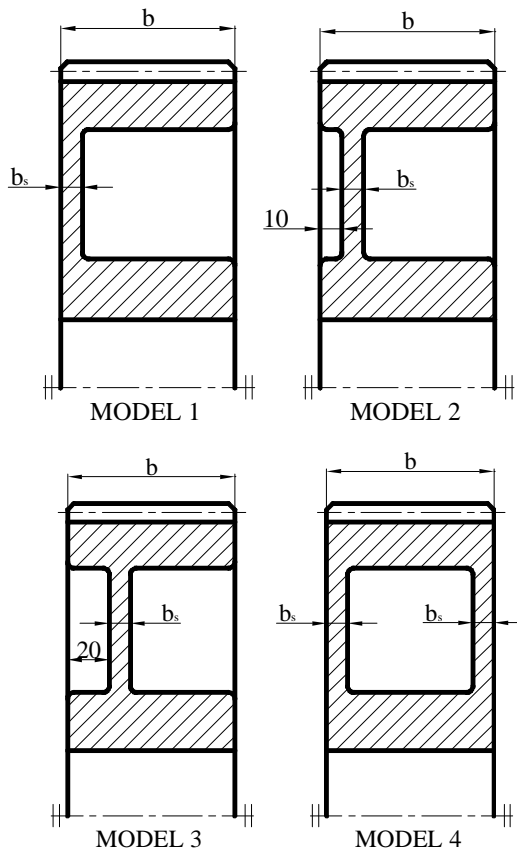


Figure 6 The locality of wheel web

The influence of the wheel web (value b_s -Figure 2) localization on the tooth stiffness will be determined on the spur gear with a number of teeth of $z=61$ and a module $m_n=4\text{mm}$ and a tooth width $b=80\text{mm}$, the value of wheel rim is $s_R=22\text{mm}$.

The wheel web thickness is $b_s=10\text{mm}$ and its locality varies according to Figure 6.

The results of the maximum tooth deformation examined at the loading point, if the force acts on the tip of the tooth (Figure 3), for wheels web with different station locations, according to the models 01 to 04 (Figure 6), are shown in the Figure 7. The value of the tooth deformation in the place of loading we consider the second highest value.

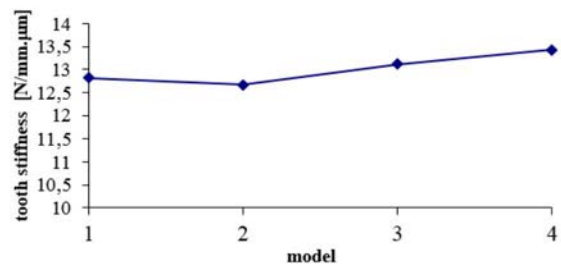


Figure 7 Influence of wheel web localization on the tooth stiffness

The minimum tooth deformation, the maximum tooth stiffness, is for the gear whit two wheel web. These wheel webs are located at the edges of the wheel width. This is due to the supportive effect of wheel web. The wheel web placement in generally is affects the teeth deformation as well as the teeth stiffness over the width of the spur gear.

5 Conclusions

Development of the modern machinery and means of production is characterized by steadily increasing performance factors in decreasing the weight of the device. Lightening of body wheel gears has affects on the deformation and stiffness of the teeth. Teeth stiffness is decreases with the decrease in thickness of the wheel rim. Teeth stiffness is not constant even after the width of tooth. If the ends of mesh contact line identic of the edge of the teeth, the teeth stiffness is less on this locality. The teeth deformation is reduced and the teeth stiffness is expanded, due to the increase in the thickness of the wheel web located at the center of the gearing width. The localization of wheel web has a influence of the teeth stiffness. Gear teeth are deformed due to the load. Recently, at ever faster evolving computer technology, the available literature, we can meet with modern numerical methods, such as finite element method (FEM), which can serve as one of the methods for the determination of teeth deformation of gearing.

DESIGN OF BODY WHEEL SHAPE TO IMPROVE TEETH STIFFNESS FOR GEARBOX OF MECHATRONIC SYSTEMS

Silvia Medvecká-Beňová; Peter Frankovský

Acknowledgement

The authors would like to thank to Slovak Grant Agency – project VEGA 1/0290/18, APVV-16-0259, VEGA 1/0473/17.

References

- [1] BATSCH, M.: Surface strength of novikovconvexo-concave gear, *Scientific Journal of Silesian University of Technology. SeriesTransport*, Vol. 90, p. 17-24, 2016.
- [2] COOLEY, Ch. G., LIU, Ch., DAI, X., PARKER, R. G.: Gear tooth mesh stiffness: A comparison of calculation approaches, *Mechanism and Machine Theory*, Vol. 105, p. 540-553, 2016.
- [3] CZECH, P.: Diagnosis of Industrial Gearboxes Condition By Vibration and Time-Frequency, Scale-Frequency, Frequency-Frequency Analysis. *Metallurgija*, Vol. 51, No. 4, p. 521-524, 2012.
- [4] SATIEPKOVÁ, A. et al: Utilizing of sensitivity analysis in preparation of optimizing procedure, *Transport*, Vol. 76, p. 32-38, 2012.
- [5] MADEJ, H., CZECH, P.: Discrete Wavelet Transform and Probabilistic Neural Network in IC Engine Fault Diagnosis, *Eksploatacja I niezawodnosć- maintenance and reliability*, Vol. 4, p. 47-54, 2010.
- [6] MEDVECKÁ-BEŇOVÁ, S.: Influence of the face width and length of contact on teeth deformation and stiffness, *Scientific Journal of Silesian University of Technology: Series Transport*, Vol. 91, p. 99-106, 2016.
- [7] RINCON, A. F., VIADERO, F., IGLESIAS, M., GARCÍA, P., SANCIBRIAN, R.: A model for the study of meshing stiffness in spur gear transmissions, *Mechanism and Machine Theory*, Vol. 61, p. 30-58, 2013.
- [8] KURYŁO, P.: Rozkład naprężeń w warstwie wierzchniej napawanych odlewów żeliwnych Proizvodstvo, *Tehnologiâ, Ekologiâ*, Vol. 10, p. 573-584, 2007. (Original in Polish)
- [9] KELEMEN, M., KELEMENOVÁ, T., JEZNÝ, J.: Four legged robot with feedback control of legs motion, *Bulletin of Applied Mechanics*, Vol. 4, No. 16, p. 115-118, 2008.
- [10] NOGA, S., MARKOWSKI, T., BOGACZ, R.: Method of determining thenormal modes of toothed gears with complex geometry, *Scientific Journal of Silesian University of Technology, SeriesTransport*, Vol. 89, p.119-127, 2015.
- [11] KAŠŠAY, P.: Comparison of pneumatic flexible shaft coupling static load characteristics obtained experimentally and by calculation, *Scientific Journal of Silesian University of Technology. SeriesTransport*, Vol. 85, No. 1925, p.57-65, 2014.
- [12] URBANSKÝ, M.: Theoretic and Experimental Determination of the Flow Resistance Coefficient at Gaseous Medium Flow into and out of the Pneumatic Coupling, *Scientific Journal of Silesian University of Technology. SeriesTransport*, Vol. 85, No. 1925, p.119-125, 2014.
- [13] KELEMEN, M., VIRGALA, I., FRANKOVSKÝ, P. et al.: Amplifying system for actuator displacement, *International Journal of Applied Engineering Research*, Vol. 11, No. 15, p. 8402-8407, 2016.
- [14] SAPIETA, M., DEKÝŠ, V., PASTOREK, P.: Using of activ thermography and lock-in method with ultrasound exication for detection of material defect, *Zeszyty naukowe Politechniki Śląskiej*, Vol. 84, No. 1907, p. 119-124, 2014.
- [15] CZECH, P., WOJNAR, G., WARCZEK, J.: Diagnostowanie uszkodzeń wtryskiwaczy w silnikach spalinowych pojazdów przy użyciu analizy bispektrum i radialnych sieci neuronowych, *Logistyka*, No. 3, p. 1181-1187, 2013. (Original in Polish)
- [16] SIKÁ, G., VELEX, P.: Analytical and numerical analysis of gears in the presence of engine acyclism, *Journal of Mechanical Design - the ASME*, Vol. 130, p. 1–6, 2008.
- [17] TERTEL, E., KURYŁO, P., PAPACZ, W.: Parallelepiped sandwich shell-searching for the optimal geometric parameters, *Applied Mechanics and Materials, Trans Tech Publications*, p. 170-174, 2014.
- [18] PIVARČIOVÁ, E., BOŽEK, P., TURYGIN, Y., ZAJAČKO, I., SHCHENYATSKY, A., VÁCLAV, Š., CÍŠAR, M., GEMELA, B.: Analysis of control and correction options of mobile robot trajectory by an inertial navigation system, *International Journal of Advanced Robotic Systems*, Vol. 15, No.1, 2018.

Review process

Single-blind peer review process.

doi:10.22306/am.v3i4.45

Received: 02 Dec. 2018

Accepted: 21 Dec. 2018

THE ASPECTS OF STRESS ANALYSIS PERFORMED BY DIGITAL IMAGE CORRELATION METHOD RELATED WITH SMOOTHING AND ITS INFLUENCE ON THE RESULTS

Martin Hagara

Technical University of Košice, Faculty of Mechanical Engineering, Department of Applied Mechanics and Mechanical Engineering, Letná 9, Slovakia, EU, martin.hagara@tuke.sk (corresponding author)

Jozef Bocko

Technical University of Kosice, Faculty of Mechanical Engineering, Department of Applied Mechanics and Mechanical Engineering, Letna 9, Kosice, Slovak Republic, EU, jozef.bocko@tuke.sk

Keywords: digital image correlation, stress analysis, smoothing, local regression, Kernel size

Abstract: The paper deals with a description of the aspects of stress analysis performed by 2D or 3D digital image correlation system. It describes the differences between the types of smoothing used in Istra4D that is a software commercially delivered with correlation systems Dantec Dynamics. The analysis was performed on flat specimen made from PSM-1 material used in photoelasticity method. By loading of the specimen in form of three-point bending, a proper dependence between the facet size set for correlation of the images and level of local regression filter (characterized by a kernel size) was found. The finding for mentioned dependence was realised by comparison of the results with the results obtained numerically in Ansys Workbench 17.0.

1 Introduction

The full-field deformation/stress analysis performed by digital image correlation method requires the use of one or more digital camera(s) with image resolution adequate to realized measurement. While the specimens of common sizes (in range from several mm² to several m²) are mostly analysed using standard digital image correlation systems consisting CCD cameras with image resolution of several Mpx, the analysis of micro-objects are performed by specially design correlation systems similar to microscopes. Correlation system consisting in one camera (Figure 1) theoretically suffices for the analysis of plane deformation [1-3].

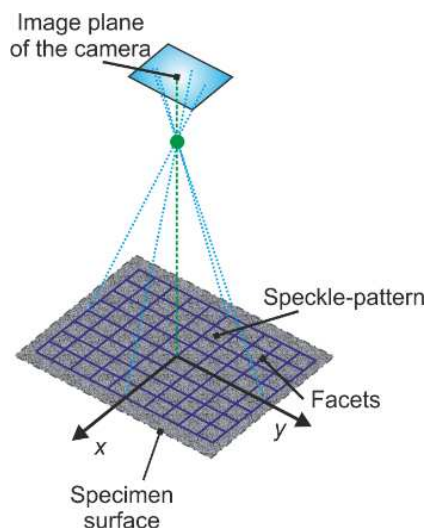


Figure 1 The scheme of single-camera (2D) correlation system

In case of spatial deformation analysis, the correlation system has to contain more cameras (Figure 2). While the concurrent between the image plane of single-camera system and the analysed specimen surface leads to the occurrence of some correlation errors, the use of more-cameras system (even in case of 2D analysis) overcomes this drawback [1-3].

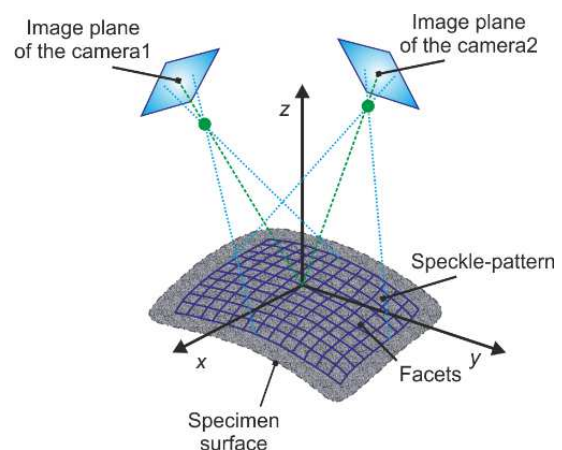


Figure 2 The scheme of two-camera (3D) correlation system

Already two-camera system can be used for analysis of the specimens with curved surface. For a purpose of high accuracy and reliability of the results, the four-camera system is able to realize both-sided deformation analysis of flat specimens and the eight-camera system (Figure 3) manages to evaluate the cylindrical shaped object along its circumference.

THE ASPECTS OF STRESS ANALYSIS PERFORMED BY DIGITAL IMAGE CORRELATION METHOD RELATED WITH SMOOTHING AND ITS INFLUENCE ON THE RESULTS

Martin Hagara; Jozef Bocko

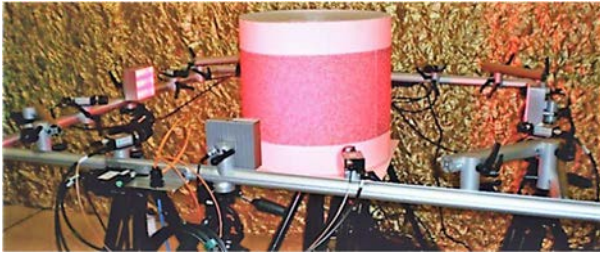


Figure 3 The configuration of eight-camera system

Digital image correlation method is based on the correlation of the digital images captured during specimen loading. It is performed along small picture elements called facets. Commonly, the facet is a group of pixels with squared shape and size from 15x15 px up to 30x30 px, however, the facet size can be adapted (increased or decreased) due to the type of the analysis. To perform proper correlation of the images, it is necessary to ensure the uniqueness of the facets, i.e. each facet has to contain unique distribution of the pixels with different level of grey value. The facets can touch or overlay themselves, but the gap between them is not possible. As the information about the displacements of the analysed object are obtained in nodal points of so-called virtual grid (the middles of the facets), the overlay of the facets (see Figure 4) belongs to the ways how to improve the image resolution, i.e. to obtain more data points and thus to copy the surface in better way.

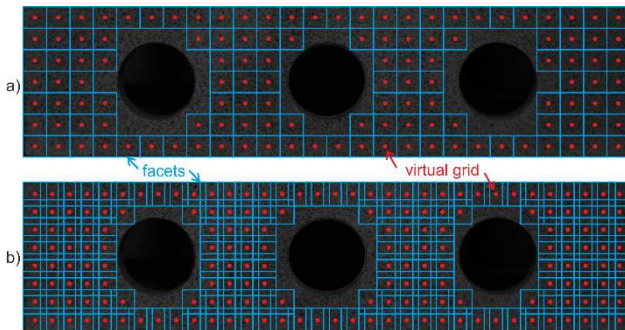


Figure 4 a) Facets without overlay, b) Facets with overlay

The manufacturer of correlation systems Dantec Dynamics recommends overlying the facets up to 1/3 of the facet size, because by such overlay the data points are still independent [4, 5]. The bigger overlay causes, that the neighboring data points lose independence. The similar situation occurs, if the smoothing filter is applied on the data. The higher level of overlying, the higher the level of smoothing as well as the number of data points used for smoothing. However, the determination of more data, or even higher image resolution does not occur. The last, simplest way for the image resolution increasing is the decreasing of facet size, however, it is limited by the quality (finesness) of the speckle-pattern created on the analysed object surface.

The results of deformation analysis performed by Dantec Dynamics correlation systems are relatively much influenced by a level of smoothing chosen by the user of software Istra4D, which is control and test software of mentioned correlation systems. The software allows filtering the data using two functions. The first one, called *Smoothing spline*, works globally on the data points and serves mainly for investigation of areas with homogeneously distributed deformation. This function fits the object surface by the bi-cubic smoothing function, whereby it uses two boundary conditions for the calculation of the spline functions. The first spline function minimizes the difference between the data point and the spline function and the second one minimizes the integral of curvature of all spline functions. In case of using this type of smoothing, two parameters are set in Istra4D – the *Grid Reduction Factor* (GRF) and the *Smoothness factor* (SF). If the GRF is increasing, the amount of measuring points is reduced and thus the obtained data are smoothed. The SF influences the condition of surface smoothing – the higher this value is, the more filtered the data are. Based on the analysis performed by manufacturer of Dantec Dynamics correlation systems, the following enclosures and recommendations for smoothing of object contour, displacements or strains using *Smoothing spline* were accepted [5]:

- SF has the biggest influence on the filtering of contour and displacements,
- by the displacement analysis oversized SF causes the higher level deviations – it smooths the whole surface and thus the noise or artefacts located in one part can affect the filtered data in another part,
- by the strain analysis oversized SF causes the devaluation of the results on the object edges,
- GRF has much lower influence on the results of displacement and strain analysis as SF.

The default levels of mentioned factors are GRF = 2.0 and SF = -1.0. The recommended range of particular factor levels for the specimen with big or small gradient of the contour, displacements and strains is given in Table 1.

Table 1 The recommended settings for GRF and SF [5]

	GRF		SF	
	Big gradient	Small gradient	Big gradient	Small gradient
Contour	2.0-2.5	≤ 3,0	-1,0-(-0,5)	≤ 0,0
Displ.	2.0	2.0	ca. -0,5	≤ 0,0
Strains	2.0	2.0	ca. -0,5	≤ 0,0

The second type of filtering used in Istra4D is *Local regression*, which fits the 2D polynomial object surface to 3rd order in the data. It is the type of smoothing optimized for keeping of local extremes and essentially determined for smoothing of non-homogenous fields (the analysis of the specimen with stress concentrators, crack initiation, etc.). Depending of the kernel size, set by the user, it is possible to define the level as well as the type of

THE ASPECTS OF STRESS ANALYSIS PERFORMED BY DIGITAL IMAGE CORRELATION METHOD RELATED WITH SMOOTHING AND ITS INFLUENCE ON THE RESULTS

Martin Hagara; Jozef Bocko

displacements and strains smoothing. While this filter is not activated, the strain is calculated from the deformation of the facet. On the other hand, the higher the kernel size, the higher the influence of deformation gradient for calculation of strains. Practically, by the set of kernel size bigger than 7×7 , the strain is determined just from the deformation gradient. As can be seen in Figure 5 and Figure 6, where the typical differences obtained by the use of both smoothing filters are depicted, it is necessary to pay attention by the choice of adequate type and level of smoothing. According to the information available for authors, there is no rule, how to set the adequate kernel size by the evaluation of the experiments using local regression filter in Istra4D.

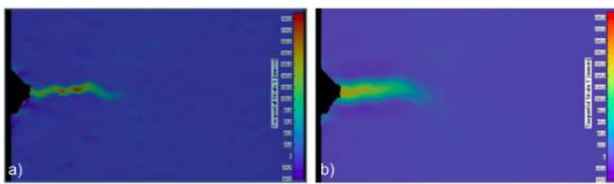


Figure 5 Smoothing of strain field with local concentrator using: a) local regression, b) smoothing spline [5]

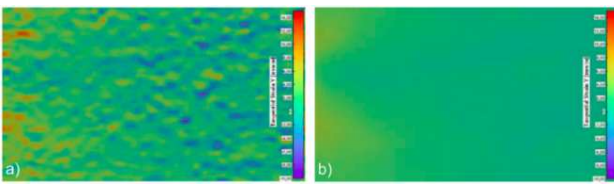


Figure 6 Smoothing of homogeneous strain field using: a) local regression, b) smoothing spline [5]

2 Experimental assessment of proper level of local regression

From mentioned reasons an analysis was performed with aim to find a dependence between the facet size and corresponding kernel size in such way, that the results of the analysis reached towards the expected results as small difference as possible. Although the authors' workplace disposes of several full-field experimental techniques (digital image correlation, electronic speckle-pattern interferometry as well as photoelasticity) it is not easy to find such method, which can serve for effective comparison of the results of strain/stress analysis on bigger surface. Although the results from experimental modelling are often used for verification of the numerical models, in some cases this process can be inversed.

The size and the shape of the analysed specimen (Figure 7) as well as the boundary conditions of the analysis were chosen with a purpose to:

- use the image resolution of low-speed CCD cameras of the correlation system Q-400 Dantec Dynamics as effectively as possible,
- have possibility to create proper speckle-pattern on the object surface, for which it will be possible

to perform correlation of the images with sufficient range of chosen facet sizes,

- reach sufficient level of deformation in the surrounding of the stress concentrators even in laboratory conditions.

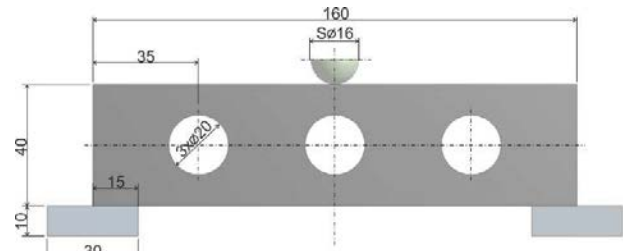


Figure 7 Shape and dimensions of the analysed specimen

The specimen was made from PSM-1 material with thickness of 10 mm, used in photoelasticity method. It was put into the loading frame, allowing the realisation of three-point bending test and loaded in such way that the displacement of the sphere-shaped spike reached 1.5 mm in the last loading step. For a purpose to minimize the potential of errors, the analysis was repeated three-times using single-camera and two-camera correlation system.

The reference images captured by both mentioned correlation systems with marked evaluation mask can be seen in Figure 8. The pixel density for 2D analysis was ca. 14.5 px/mm and for 3D analysis ca. 14.64 px/mm.

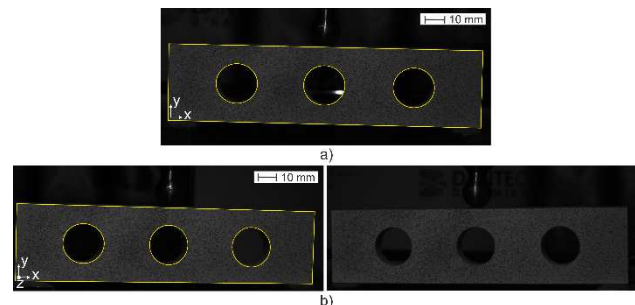


Figure 8 Reference images captured by: a) single-camera system, b) two-camera system

Numerical model consists in four bodies – the analysed specimen made from PSM-1 material with Young's modulus $E = 2.5 \text{ GPa}$ and Poisson ratio $\mu = 0.38$, two supports and the hemispheric spike made from stainless steel ($E = 200 \text{ GPa}$ and $\mu = 0.3$). The supports were located in such way that they supported the specimen on the areas of size $15 \times 10 \text{ mm}^2$ (see Figure 7). The loading was realized by the movement of the spike in the direction of vertical specimen axis of symmetry. The contact of two rigid bodies with friction coefficient 0.4 (the value used for friction between steel and polycarbonate) were defined between corresponding parts of the model. The mesh of finite elements, created on particular parts of the numerical

THE ASPECTS OF STRESS ANALYSIS PERFORMED BY DIGITAL IMAGE CORRELATION METHOD RELATED WITH SMOOTHING AND ITS INFLUENCE ON THE RESULTS

Martin Hagara; Jozef Bocko

model, together with defined boundary conditions can be seen in Figure 9.

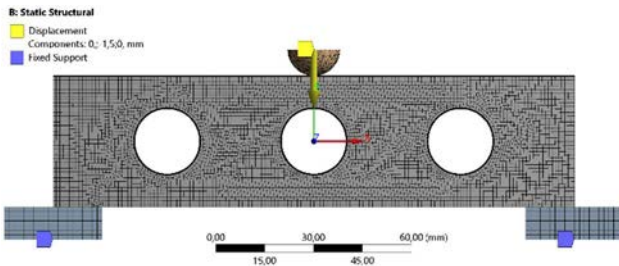


Figure 9 The finite element mesh with the boundary conditions defined at the numerical model

Figure 10 shows the distribution of equivalent von Mises stress on the analysed specimen surface. The best way, how to compare the results from both analyses would be to export nodal data from FEA and to couple them with corresponding experimental nodal data from the middles of the facets. Although, Istra4D allows to export data in hierarchical HDF5 file format, it is complicated to couple the mentioned data properly, because neither the amounts, nor the locations of nodal points have to correspond. For that reason, the authors decided to compare the values of equivalent stress on two corresponding areas with sizes 90x6 mm² (see Figure 11), which the highest levels of stresses were determined on.

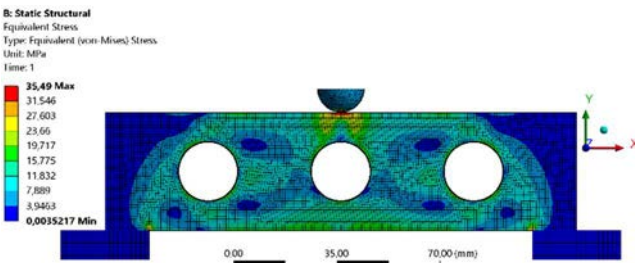


Figure 10 Equivalent von Mises stress field obtained on the analysed specimen surface

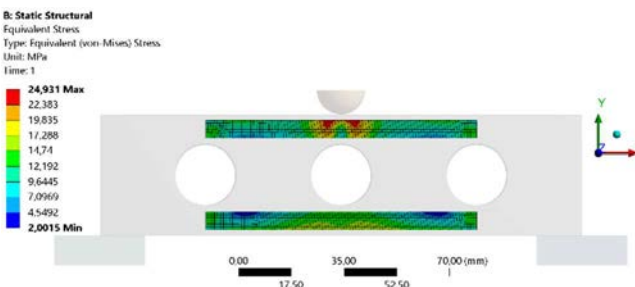


Figure 11 Two areas defined for comparison of equivalent von Mises stress determined by DIC and FEA

The height of the areas lower than 10 mm (by which the areas could touch the bottom or the upper edge of the specimen) was chosen with a purpose that digital image correlation allows to obtain data just in the middles of the facets. This fact leads to the loss of the data on the edges – the distance of first data point from the edge is minimally one half of the facet size.

The measurements realized using single-camera and two-camera system were evaluated in sequence using different facet sizes. In case that the facets touch themselves, the facet sizes used for correlation of the images were in the range from 10x10 px up to 25x25 px. In case of their overlay, the facet sizes were chosen in range from 10x10 px up to 30x30 px. Subsequently, the various levels of smoothing were set to filter the data and to find the best equality between the results obtained numerically and experimentally. There were two criterions for best equality. If the functions expressed by eq. (1) and eq. (2)

$$\Delta_{\sigma_{\max}} = \frac{\sum_{i=1}^3 \text{abs} \left(\left(\frac{\max(\sigma_{i_{\text{exp}}}^{\text{Mises}})}{\max(\sigma_{i_{\text{num}}}^{\text{Mises}})} - 1 \right) \cdot 100 \right)}{3} \quad (1)$$

$$\Delta_{\sigma_{\text{str}}} = \frac{\sum_{i=1}^3 \text{abs} \left(\left(\frac{\text{mean}(\sigma_{i_{\text{exp}}}^{\text{Mises}})}{\text{mean}(\sigma_{i_{\text{num}}}^{\text{Mises}})} - 1 \right) \cdot 100 \right)}{3} \quad (2)$$

where $i=1,2,3$ are three performed measurements, $\max(\sigma_{i_{\text{exp}}}^{\text{Mises}})$ and $\text{mean}(\sigma_{i_{\text{exp}}}^{\text{Mises}})$ are the maximal and the mean values obtained on the analyzed areas experimentally by digital image correlation system, $\max(\sigma_{i_{\text{num}}}^{\text{Mises}})$ and $\text{mean}(\sigma_{i_{\text{num}}}^{\text{Mises}})$ are the maximal and the mean values obtained on the analysed areas experimentally by software Ansys Workbench 17.0, reached minimum the optimal kernel size was found.

The bar graphs in Figures 12-15 show the determined optimal dependence between the facet size used for correlation of the images captured by single- or two-camera system and the kernel size of the local regression used for smoothing of the data. The obtained dependences indicate that the settings of kernel size should be approximately the same for 2D as well as 3D analysis.

THE ASPECTS OF STRESS ANALYSIS PERFORMED BY DIGITAL IMAGE CORRELATION METHOD RELATED WITH SMOOTHING AND ITS INFLUENCE ON THE RESULTS

Martin Hagara; Jozef Bocko

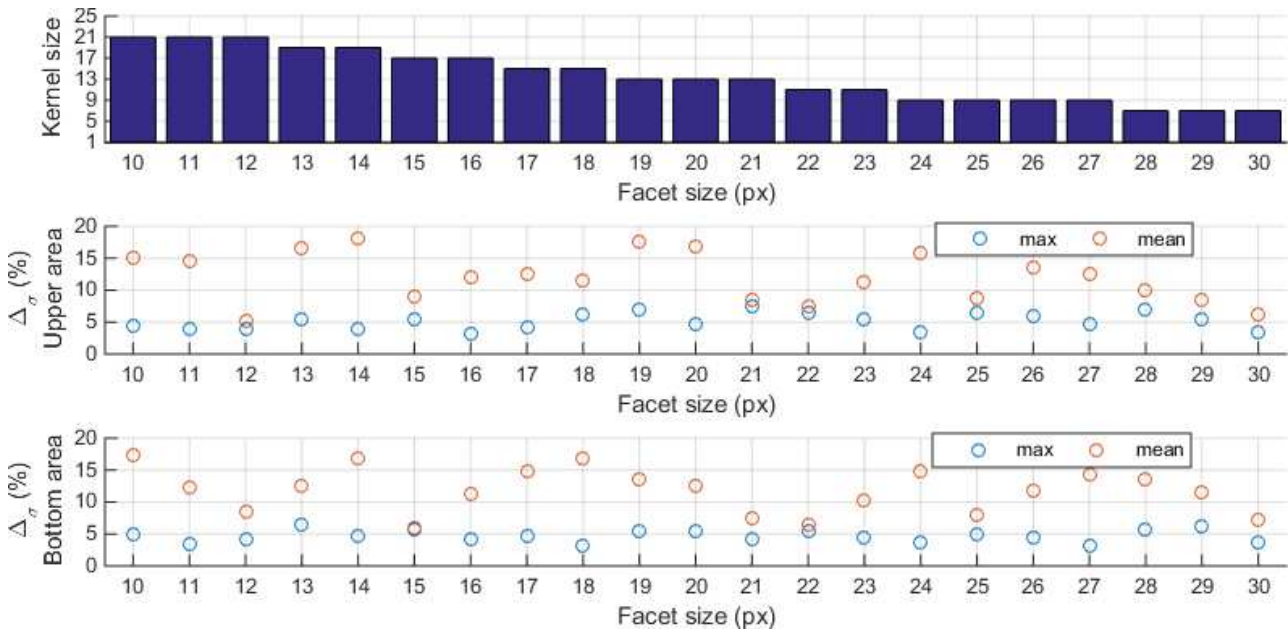


Figure 12 Dependence between the facet size and corresponding level of kernel size used for smoothing of 2D analysis without overlay of the facets (the first graph), corresponding differences in maximal and mean value of equivalent stress obtained on analysed areas (the second and the third graph)

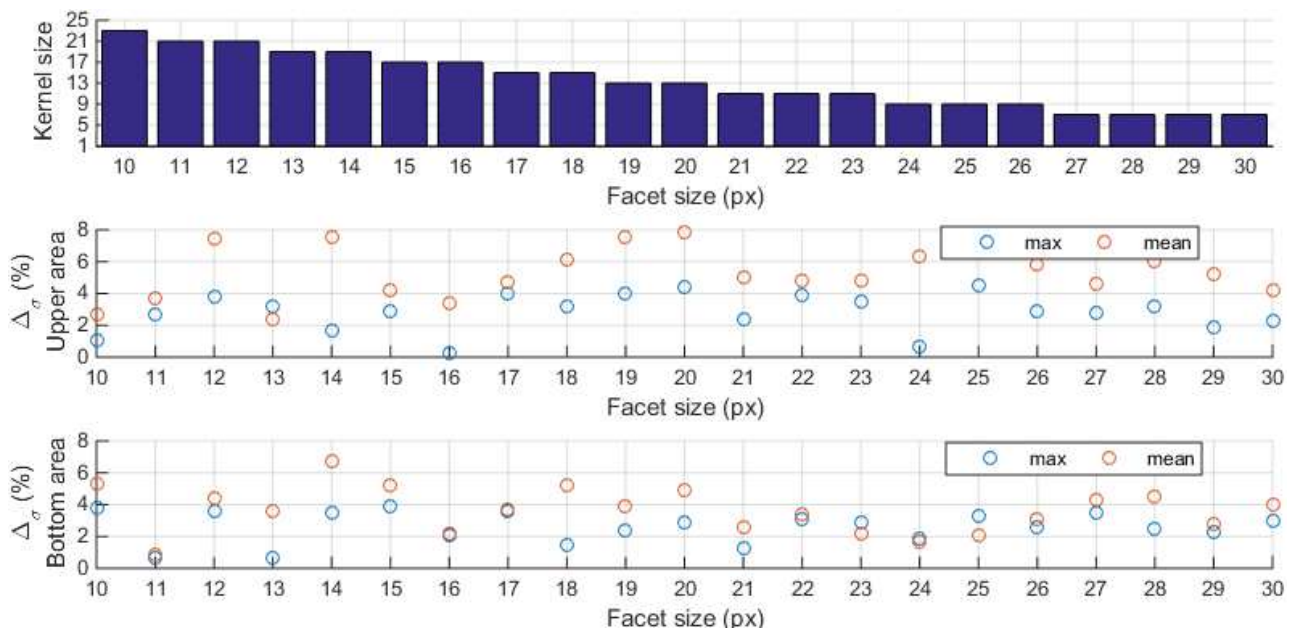


Figure 13 Dependence between the facet size and corresponding level of kernel size used for smoothing of 3D analysis without overlay of the facets (the first graph), corresponding differences in maximal and mean value of equivalent stress obtained on analysed areas (the second and the third graph)

THE ASPECTS OF STRESS ANALYSIS PERFORMED BY DIGITAL IMAGE CORRELATION METHOD RELATED WITH SMOOTHING AND ITS INFLUENCE ON THE RESULTS

Martin Hagara; Jozef Bocko

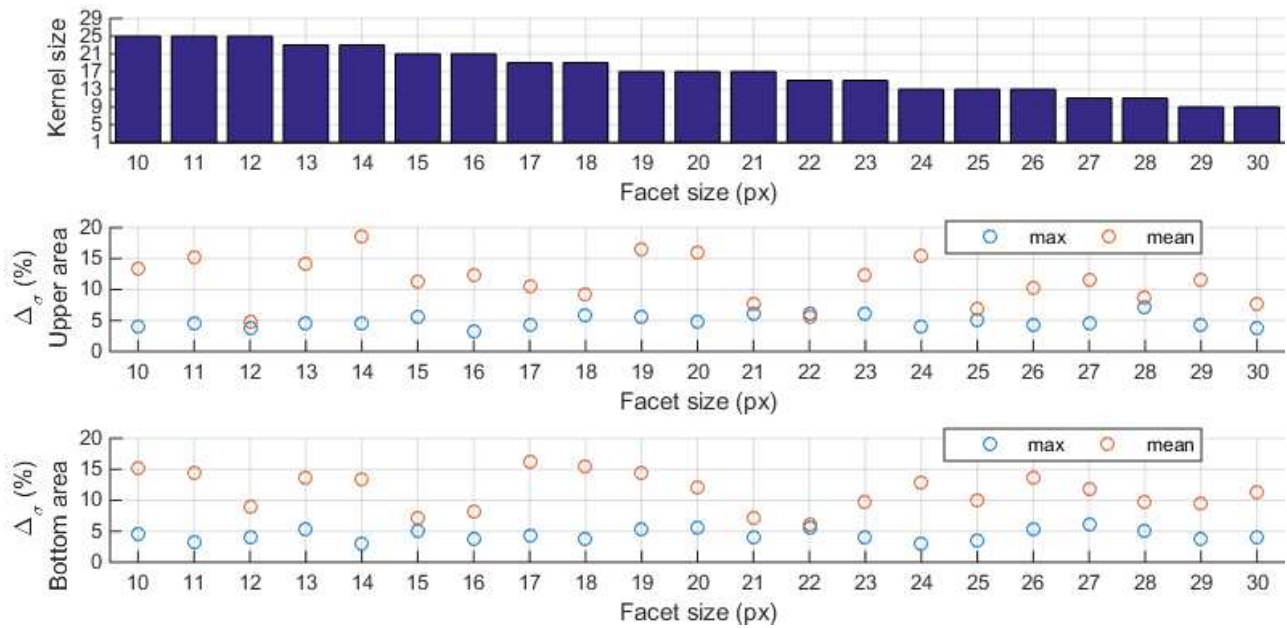


Figure 14 Dependence between the facet size and corresponding level of kernel size used for smoothing of 2D analysis with overlay of the facets (the first graph), corresponding differences in maximal and mean value of equivalent stress obtained on analysed areas (the second and the third graph)

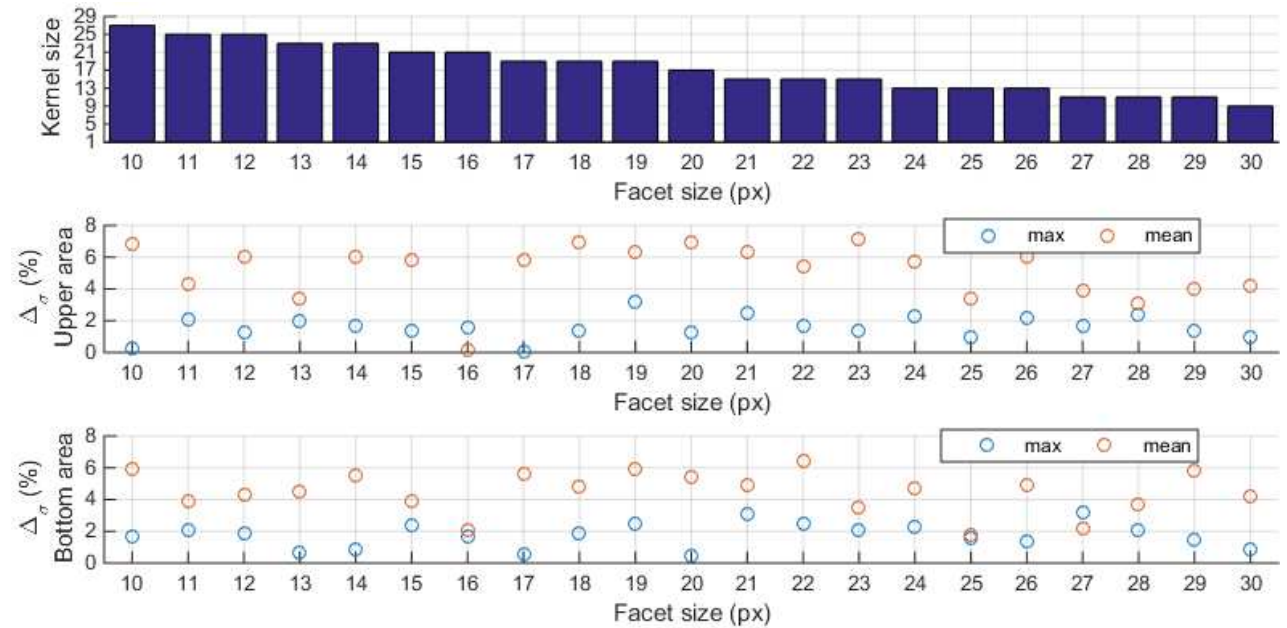


Figure 15 Dependence between the facet size and corresponding level of kernel size used for smoothing of 3D analysis with overlay of the facets (the first graph), corresponding differences in maximal and mean value of equivalent stress obtained on analysed areas (the second and the third graph)

The differences in the results obtained by the correlation of the facets without as well as with overlay are not very significant. By the use of single-camera system, the higher differences from the results obtained numerically can be observed. According to the authors this phenomenon was caused by the decay of parallelism between the camera image plane and object surface during loading of the specimen. Although the authors tried to ensure the plane deformation of the specimen, in some

cases it is not so easy to reach it that leads to occurring of reconstruction errors.

The advantage of the use of facets with overlay accrues from the course depicted in Figure 16, which depicts the dependence of correlated facets amount on the facet size registered in 3D analysis.

THE ASPECTS OF STRESS ANALYSIS PERFORMED BY DIGITAL IMAGE CORRELATION METHOD RELATED WITH SMOOTHING AND ITS INFLUENCE ON THE RESULTS

Martin Hagara; Jozef Bocko

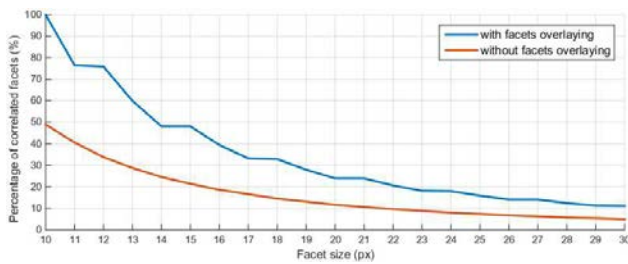


Figure 16 Dependence of percentage of correlated facets on the facet size used for evaluation with and without overlay of the facets

In this case, the 100% value corresponds to the value of correlated 22609 facets with size of 10x10 px and overlay of 33%. As can be seen the image resolution by the use of facets without overlay is approximately 2x smaller.

Figure 17 and Figure 18 depict the equivalent von Mises stress field evaluated by the smallest image resolution (the overall amount of evaluated facet with size of 30x30 px without facets overlay was 1122) as well as by the biggest image resolution (the overall amount of evaluated facet with size of 10x10 px with facets overlay was 22609).

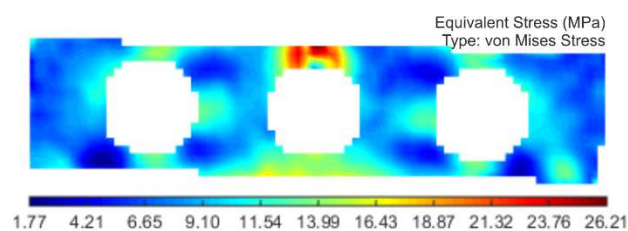


Figure 17 Equivalent von Mises stress obtained on the analysed specimen surface by the correlation with the facets size equal to 30x30 px without overlay

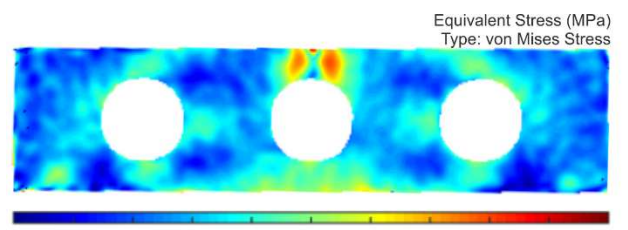


Figure 18 Equivalent von Mises stress obtained on the analysed specimen surface by the correlation with the facets size equal to 10x10 px with overlay

Although the criterions defined by eq. (1) and eq. (2) for facet size 30x30 px without overlay reached relatively favourable values, the distribution of von Mises stress field (see Fig. 17) is in the central upper part of the specimen influenced by small number of data points. Compared to mentioned fact, the von Mises stress field depicted in Fig. 18 shows good equality to the results obtained numerically. Moreover, it copies the object surface in better way and thus the maximal values of stress differ less from the maximal values of finite elements analysis.

3 Conclusions

The authors describe the aspects corresponding with the use of 2D and 3D digital image correlation system in stress analysis of flat specimen. It can be stated, that the use of two-camera system allows stress analysis with smaller risk of reconstruction errors that leads to results with higher accuracy. In the paper, the dependence between the facet size used for correlation of the images and the optimal kernel size used in local regression filter was found. If it is possible the authors recommend to use overlaid facets, which ensure obtaining data as near to the object edges as possible. Moreover, the images has higher image resolution, that increase the quality of the obtained results.

Acknowledgement

The paper is the result of project implementation VEGA 1/0731/16.

References

- [1] SIEBERT, T., SPLITTHOF, K., STECKLUM, S., HERBST, CH.: *New features in digital image correlation techniques*, 22nd DANUBIA-ADRIA Symposium on Experimental Methods in Solid Mechanics, 2005.
- [2] SUTTON, M.A., ORTEU, J.-J., SCHREIER, H.W.: *Image Correlation for Shape, Motion and Deformation Measurements: Basic Concepts, Theory and Applications*, 1st ed., New York, Springer Science & Business Media, 2009.
- [3] TREBUŇA, F., HUŇADY, R., HAGARA, M.: *Experimental methods of mechanics – Digital image correlation (in Slovak)*, 1st ed., Košice, TUKE, 2015.
- [4] DANTEC DYNAMICS: Q-400 User Manual, 2012.
- [5] DANTEC DYNAMICS: Influence of Filter parameter on Q-4xx measurement results, Technical note, 2001.

Review process

Single-blind peer review process.



JOURNAL STATEMENT

Journal name:	Acta Mechatronica
Abbreviated key title:	Acta Mechatron
Journal title initials:	AM
Journal doi:	10.22306/am
ISSN:	2453-7306
Start year:	2016
The first publishing:	March 2016
Issue publishing:	Quarterly
Publishing form:	On-line electronic publishing
Availability of articles:	Open Access Journal
Journal license:	CC BY-NC
Publication ethics:	COPE, ELSEVIER Publishing Ethics
Plagiarism check:	Worldwide originality control system
Peer review process:	Single-blind review at least two reviewers
Language:	English
Journal e-mail:	info@actamechatronica.eu

The journal focuses mainly on original, interesting, new and quality, theoretical, practical and application-oriented contributions to the scientific fields and research as well as to pedagogy and training in mechatronics.

Publisher:	4S go, s.r.o.
Address:	Semsa 24, 044 21 Semsa, Slovak Republic, EU
Phone:	+421 948 366 110
Publisher e-mail:	info@4sgo.eu

**Responsibility for the content of a manuscript rests upon the authors
and not upon the editors or the publisher.**